

Anatomy of electrical signals and dc-voltage line shape in spin-torque ferromagnetic resonanceYin Zhang,^{1,2} Q. Liu,³ B. F. Miao,^{3,4} H. F. Ding,^{3,4,*} and X. R. Wang^{1,2,†}¹*Physics Department, The Hong Kong University of Science and Technology, Clear Water Bay, Kowloon, Hong Kong*²*HKUST Shenzhen Research Institute, Shenzhen 518057, China*³*National Laboratory of Solid State Microstructures and Department of Physics, Nanjing University, 22 Hankou Road, Nanjing 210093, China*⁴*Collaborative Innovation Center of Advanced Microstructures, Nanjing University, 22 Hankou Road, Nanjing 210093, China*

(Received 30 October 2018; revised manuscript received 25 December 2018; published 19 February 2019)

The electrical detection of spin-torque ferromagnetic resonance (st-FMR) is becoming a popular method for measuring the spin-Hall angle of heavy metals (HM). However, various sensible analysis on the same material with either the same or different experimental setups yielded different spin-Hall angles with large discrepancy, indicating some missing ingredients in our current understanding of st-FMR. Here we carry out a careful analysis of electrical signals of the st-FMR in a HM/ferromagnet (HM/FM) bilayer with an arbitrary magnetic anisotropy. The FM magnetization is driven by two radio-frequency (rf) forces: the rf Oersted field generated by an applied rf electric current and the so called rf spin-orbit torque from the spin current flowing perpendicularly from the HM to the FM due to the spin-Hall effect. By using the universal form of the dynamic susceptibility matrix of magnetic materials at the st-FMR, the electrical signals, originated from the anisotropic magnetoresistance, anomalous Hall effect, and inverse spin-Hall effect are analyzed and dc-voltage line shapes near the st-FMR are obtained. Angular dependence of dc voltage is given for two setups. A way of experimentally extracting the spin-Hall angle of a HM is proposed.

DOI: [10.1103/PhysRevB.99.064424](https://doi.org/10.1103/PhysRevB.99.064424)**I. INTRODUCTION**

Ferromagnetic resonance (FMR) is a traditional method for extracting magnetic material parameters such as magnetization, magnetic anisotropy and damping coefficient [1–13] by either measuring microwave absorption or detecting electrical signals [14–37]. The microwave absorption spectroscopy is the first generation of FMR technique. It typically requires large samples in order to have detectable absorption signal. The analysis is relatively simple because it uses the field dependence of the FMR peak and the peak width to probe the magnetization and damping. In the electrical detection of FMR, sample sizes can be very small due to the high sensitivity of electrical signal detection. Its analysis is, however, more involving although electrical detection can be at very high precision and samples have less effect on microwave fields. The electrical signals can come from the anisotropic magnetoresistance (AMR), anomalous Hall effect (AHE) [14–16], as well as the recently discovered inverse spin-Hall effect (ISHE) [38–43]. This technique has been widely used in recent years to extract the spin-Hall angle of heavy metals that measures the spin-charge interconversion efficiency in both the spin-Hall effect (SHE) and ISHE [17–29]. The spin Hall angle of a heavy metal (HM) is typically measured from the HM/ferromagnet (HM/FM) bilayers. The FM can be a metal or an insulator. The FMR is triggered by a microwave in cavity or coplanar waveguide [16–18,20,26–30]. The typical setup in an FMR is to eliminate effect of the microwave electric field

on magnetization dynamics so that microwave magnetic field is assumed to be the only driving force of the FMR. So far, the experimentally extracted values show a large discrepancy for the same materials even with similar experimental setups. For example, the measured spin-Hall angle of Pt varies from 0.013 to 0.08 [20–26,36]. This large discrepancy comes from many different sources although it is often attributed to the inaccuracy in mixing conductance of HM/FM interface and spin diffusion length of the HM. For example, the dynamic susceptibility at the FMR is in general a non-Polder tensor [35] that depends on the magnetic anisotropy and damping constant, but it is commonly treated as scalar numbers or at most a Polder tensor in experimental analysis. Also, the electrical signal is very sensitive to the phase difference between rf magnetic and electric fields inside a sample [16,26,28,35]. This phase difference is not easy to determine accurately in experiments. In general, the analysis for both HM/FM-metal and HM/FM-insulator are complicated. For metallic FM, one needs to separate the contribution of ISHE from those of AMR and AHE through a very careful analysis in an experimental setup [17–24,26,28,29,35]. Although there is no electrical signal in an insulator so that no AMR and AHE contributions to dc voltage from the FM insulator, the amount of spin current pumped from FM through the HM/FM interface is an issue, in particular when new effects like the spin-Hall magnetoresistance is considered [44–46].

In recent years, the spin-torque ferromagnetic resonance (st-FMR) is becoming another popular method for measuring spin-Hall angle where an rf current is directly applied in the sample [21–24]. In this technique, there are two driving forces. One is rf Oersted field generated from rf current applied in the bilayer. The other is so-called the rf spin-orbit

*Corresponding author: hfding@nju.edu.cn†Corresponding author: phxwan@ust.hk

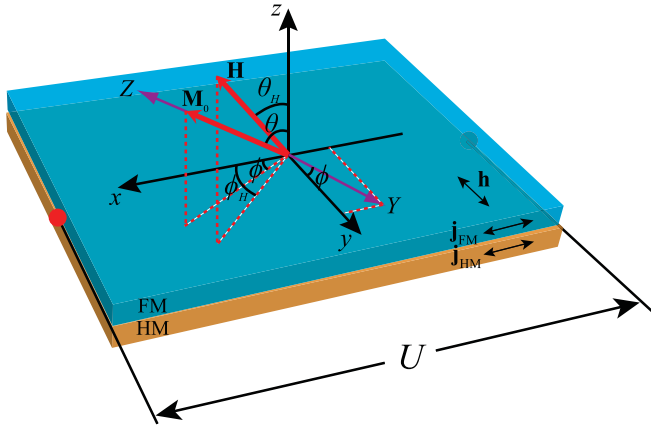


FIG. 1. Model system that mimics the experimental setups of st-FMR. The xyz coordinate is fixed with respect to the sample. The HM/FM bilayer sample lies in the xy plane. The XYZ is a moving coordinate with the Z axis along \mathbf{M}_0 and the Y axis in the xy plane. θ and ϕ are the polar and azimuthal angles of \mathbf{M}_0 in the xyz coordinate, i.e., θ is the angle between the Z and z axes and ϕ is the angle between the in-plane component of \mathbf{M}_0 and the x axis. θ_H and ϕ_H are the polar and azimuthal angles of the external static magnetic field \mathbf{H} in the xyz coordinate. \mathbf{j}_{FM} and \mathbf{j}_{HM} are, respectively, the rf electric current in the FM and HM layers.

torque (SOT) from the spin current flowing perpendicularly from the HM to the FM due to SHE. The magnetization can resonate with both rf Oersted field and the rf SOT. Compare with microwave FMR, st-FMR does not have phase difference problem between rf electric and magnetic fields since the Oersted field is in-phase with rf current. However, the spin-Hall angle was often overestimated [20–24,26], which indicates some missing ingredients in our current understanding of st-FMR. Thus a careful analysis of electrical signals of the st-FMR is timely important.

In this work, we perform an anatomy of electrical signals and dc-voltage line shape in st-FMR. The paper is organized as follows. In Sec. II, we first describe the model and approach adopted in this study. By using the universal form of the dynamic susceptibility matrix of magnetic materials at FMR, we analyze the electrical signals originated from AMR, AHE, and ISHE, and obtain the dc-voltage line shape near the st-FMR. A recipe for extracting the spin-Hall angle of the HM from the experiments is proposed. In Sec. III, the theoretical angular dependence of dc voltage is obtained for two experimental configurations. In the discussion, based on general physics principles, we argue possible new SHEs and ISHEs in magnetic materials when the charges, spins, and orbits mutually interact among themselves. The conclusion is given in Sec. IV, followed by Acknowledgments.

II. THEORETICAL ANALYSIS

A. Model and analysis

1. Setup and magnetization dynamics

The st-FMR model consists of a HM/FM bilayer lying in the xy plane, as shown in Fig. 1. \mathbf{M} is the magnetization of FM. A static magnetic field \mathbf{H} together with an rf current

density $\mathbf{J}_a = \text{Re}(\mathbf{j}_a e^{-i\omega t})$ ($a = \text{FM}, \text{HM}$) is applied in the bilayer where ω is the microwave frequency. Without the rf current, the magnetization is along \mathbf{M}_0 . To simplify the analysis, we use two Cartesian coordinates. The xyz coordinate is fixed with respect to the sample while the XYZ is a moving coordinate with the Z axis along \mathbf{M}_0 and the Y axis in the xy plane. θ and ϕ are the polar and azimuthal angles of \mathbf{M}_0 in the xyz coordinate, i.e., θ is the angle between the Z and z axes, and ϕ is the angle between the in-plane component of \mathbf{M}_0 and the x axis. θ_H and ϕ_H are the polar and azimuthal angles of the external static magnetic field \mathbf{H} in the xyz coordinate. Therefore, once \mathbf{M}_0 is determined, unit vectors \hat{Z} , \hat{X} , and \hat{Y} are, respectively, $\hat{Z} = \sin\theta \cos\phi\hat{x} + \sin\theta \sin\phi\hat{y} + \cos\theta\hat{z}$, $\hat{X} = \cos\theta \cos\phi\hat{x} + \cos\theta \sin\phi\hat{y} - \sin\theta\hat{z}$, and $\hat{Y} = -\sin\phi\hat{x} + \cos\phi\hat{y}$.

Under a microwave radiation, the rf electric current in HM generates an rf transverse spin current $\mathbf{J}_s = \text{Re}(\mathbf{j}_s e^{-i\omega t})$ perpendicularly flowing into the FM layer via the SHE [40] where the polarization $\mathbf{j}_s = (\frac{\hbar}{2e})\theta_{\text{SH}}\mathbf{j}_{\text{HM}} \times \hat{z}$. Spin-Hall angle θ_{SH} measures the conversion efficiency between charge and spin. The SOT on the magnetization induced by the spin current is [43,47,48],

$$\vec{\tau} = -\gamma \frac{a}{M} \mathbf{M} \times (\mathbf{M} \times \mathbf{J}_s) + \gamma \beta a \mathbf{M} \times \mathbf{J}_s, \quad (1)$$

where the first term on the right-hand side is the Slonczewski-like torque, while the second term is the fieldlike torque. $a = \frac{1}{d_{\text{FM}}\mu_0 M} \eta$, where d_{FM} and μ_0 are, respectively, the thickness of the FM layer and the permeability constant. η measures the efficiency of spin angular momentum transfer from the spin current to the magnetization. β measures the fieldlike torque and can be an arbitrary real number since this torque may also be directly generated from the Rashba effect [43].

The magnetization dynamics under a microwave radiation is governed by the generalized Landau-Lifshitz-Gilbert (LLG) equation [49],

$$\frac{\partial \mathbf{M}}{\partial t} = -\gamma \mathbf{M} \times \mathbf{H}_{\text{eff}} + \frac{\alpha}{M} \mathbf{M} \times \frac{\partial \mathbf{M}}{\partial t} + \vec{\tau}, \quad (2)$$

where γ is the gyromagnetic ratio, α is the Gilbert damping coefficient, and \mathbf{H}_{eff} is the effective field which includes the applied static magnetic field \mathbf{H} , rf Oersted field $\text{Re}(\mathbf{h} e^{-i\omega t})$ generated by the rf current in the system and anisotropy field. We assume that the microwave skin depth is much larger than the FM thickness d_{FM} , so that the rf current \mathbf{j}_{FM} in the FM layer is spatially uniform and the Oersted field from \mathbf{j}_{FM} produces no net torque on magnetization. Therefore, the rf Oersted field is only from \mathbf{j}_{HM} . Under the condition that the sample width is much larger than the HM thickness d_{HM} , the rf magnetic field can be determined by the Ampere's law, i.e., $\mathbf{h} = \frac{d_{\text{HM}}}{2} \mathbf{j}_{\text{HM}} \times \hat{z}$.

In the linear response regime, $\mathbf{M} = \mathbf{M}_0 + \text{Re}(\mathbf{m} e^{-i\omega t})$ will deviate from its static value \mathbf{M}_0 by a small amount under the rf Oersted field \mathbf{h} and rf SOT $\vec{\tau}$ of frequency of ω . They are from the same physical origin as rf SOT is originated from the rf spin current that converted from j_{HM} via SHE. Although the sources of the rf Oersted field \mathbf{h} and rf SOT are the same, it is convenient to consider them as two separated forces of magnetization. Off the resonance, the magnitude of \mathbf{m} is negligibly small so that no detectable electrical signal

exists. Near the resonance, the responses of \mathbf{m} to rf field \mathbf{h} and rf \mathbf{e} (or rf SOT) are large and are characterized by the dynamic susceptibilities $\vec{\chi}$ and $\vec{\kappa}$ defined as $\mathbf{m} = \vec{\chi}\mathbf{h} + \vec{\kappa}\mathbf{e}$. \mathbf{e} generates \mathbf{j}_{HM} that is the ultimate source of \mathbf{h} and rf SOT. Thus $\vec{\kappa}$ and $\vec{\chi}$ are related to each other (see the next section).

2. Origins of dc voltage

In a magnetic field, \mathbf{m} and \mathbf{j}_{FM} , as well as \mathbf{j}_{HM} , are not in phase because $\vec{\kappa}$ and $\vec{\chi}$ are complex tensors. Thus \mathbf{j}_{FM} feels an oscillating resistance due to AMR and AHE that has a phase lag with \mathbf{j}_{FM} , resulting in spin rectification effect. The phase lag also results in a dc spin current so that a dc voltage can also appear in HM from ISHE. In summary, dc voltage comes from AMR, AHE, and ISHE,

$$U = U_{\text{AMR}} + U_{\text{AHE}} + U_{\text{ISHE}}. \quad (3)$$

According to the generalized Ohm's law [35] in which the AMR and AHE couple the magnetization motion \mathbf{m} with the rf electric current \mathbf{j}_{FM} , U_{AMR} and U_{AHE} are [35]

$$U_{\text{AMR}} = \frac{\Delta\rho}{2M} \text{Re}\{[(\mathbf{j}_{\text{FM}}^* \cdot \mathbf{m})l_z + j_{\text{FM},z}^*(\mathbf{m} \cdot \mathbf{l})]\}, \quad (4)$$

$$U_{\text{AHE}} = -\frac{R_1}{2} \text{Re}[(\mathbf{j}_{\text{FM}}^* \times \mathbf{m}) \cdot \mathbf{l}], \quad (5)$$

where $\Delta\rho = \rho_{\parallel} - \rho_{\perp}$ with ρ_{\parallel} (ρ_{\perp}) being the longitudinal (transverse) resistivity of the HM/FM bilayer when \mathbf{M} is parallel (perpendicular) to \mathbf{J}_{FM} . R_1 describes the AHE of the FM, and \mathbf{l} is the displacement vector between two electrode contact points used to measure the dc voltage.

U_{ISHE} comes from the ISHE that converts a pure spin current \mathbf{J}_s , pumped by precessing magnetization near the st-FMR to a charge current. The pumped spin current \mathbf{J}_s is [27,41,42]

$$\mathbf{J}_s = \frac{\hbar}{4\pi} g_{\text{eff}}^{\uparrow\downarrow} \frac{1}{M^2} \mathbf{M} \times \frac{\partial \mathbf{M}}{\partial t}, \quad (6)$$

where $g_{\text{eff}}^{\uparrow\downarrow}$ is the effective spin mixing conductance. \mathbf{J}_s is then converted to an electric current in the HM layer,

$$\mathbf{J}_{\text{ISHE}} = -\frac{2e}{\hbar} \theta_{\text{SH}} \hat{z} \times \mathbf{J}_s, \quad (7)$$

which results in a dc voltage,

$$\begin{aligned} U_{\text{ISHE}} &= \frac{1}{\sigma_{\text{HM}}} \langle \mathbf{J}_{\text{ISHE}} \rangle \cdot \mathbf{l} \\ &= -\frac{2e}{\hbar} \frac{\theta_{\text{SH}}}{\sigma_{\text{HM}}} (\hat{z} \times \langle \mathbf{J}_s \rangle) \cdot \mathbf{l}, \end{aligned} \quad (8)$$

where $\langle \dots \rangle$ denotes the time average. From Eq. (6), the dc spin current is $\langle \mathbf{J}_s \rangle = g_{\text{eff}}^{\uparrow\downarrow} \frac{\hbar\omega}{4\pi M^2} \text{Im}(m_X^* m_Y) \hat{z}$. Thus U_{ISHE} becomes

$$U_{\text{ISHE}} = -\frac{g_{\text{eff}}^{\uparrow\downarrow} \theta_{\text{SH}} e \omega}{2\pi \sigma_{\text{HM}} M^2} \text{Im}(m_X^* m_Y) [(z \times \hat{z}) \cdot \mathbf{l}]. \quad (9)$$

According to Eqs. (4), (5), and (9), the dc voltage from the generalized Ohm's law and ISHE depend on how \mathbf{m} responds to \mathbf{h} and \mathbf{e} , or the dynamic magnetic susceptibility matrices $\vec{\chi}$ and $\vec{\kappa}$ near st-FMR.

B. Dynamic magnetic susceptibility matrix $\vec{\chi}$ and $\vec{\kappa}$

As mentioned in the last section, it is convenient to characterize the dynamical component \mathbf{m} by the dynamic susceptibilities $\vec{\chi}$ and $\vec{\kappa}$ as $\mathbf{m} = \vec{\chi}\mathbf{h} + \vec{\kappa}\mathbf{e}$, although \mathbf{j}_{HM} generated by \mathbf{e} is the ultimate source of \mathbf{h} and rf SOT. The universal form of $\vec{\chi}(\omega)$ has been obtained in our previous work [35]

$$\vec{\chi}(\omega) = \frac{\pi\Gamma}{2} [L(\omega, \omega_0, \Gamma) + iD(\omega, \omega_0, \Gamma)] \vec{C}, \quad (10)$$

where $L(\omega, \omega_0, \Gamma)$ is the Lorentzian function,

$$L(\omega, \omega_0, \Gamma) = \frac{1}{\pi} \frac{\frac{\Gamma}{2}}{(\omega - \omega_0)^2 + \left(\frac{\Gamma}{2}\right)^2}, \quad (11)$$

and the function $D(\omega, \omega_0, \Gamma)$ is

$$D(\omega, \omega_0, \Gamma) = \frac{1}{\pi} \frac{\omega - \omega_0}{(\omega - \omega_0)^2 + \left(\frac{\Gamma}{2}\right)^2}, \quad (12)$$

where ω_0 denotes the resonance frequency and Γ is the linewidth, which is a positive number. The matrix \vec{C} is

$$\vec{C} = \begin{pmatrix} iC_1 & C_3 + iC_2 & 0 \\ -C_3 + iC_2 & iC_4 & 0 \\ 0 & 0 & 0 \end{pmatrix}. \quad (13)$$

In the case that the microwave frequency ω is fixed and the applied static magnetic field H is swept, the field dependence of $\vec{\chi}$ has the following form for an arbitrary FM [35]:

$$\vec{\chi}(H) = \frac{\pi\Gamma_1}{2} [L(H, H_0, \Gamma_1) + i \frac{-\zeta}{|\zeta|} D(H, H_0, \Gamma_1)] \vec{C}(H_0), \quad (14)$$

where H_0 is the resonance field, $\zeta = \frac{d\omega_0}{dH}|_{H=H_0}$, and $\Gamma_1 = \Gamma(H_0)/|\zeta|$ is the linewidth of the field.

Because \mathbf{e} generates \mathbf{j}_{HM} that is the ultimate source of \mathbf{h} and rf SOT, $\vec{\kappa}$ and $\vec{\chi}$ are related. To find the relationship between $\vec{\kappa}$ and $\vec{\chi}$, we start from the generalized LLG equation (2), which can be recasted as

$$\frac{\partial \mathbf{M}}{\partial t} = -\gamma \mathbf{M} \times (\mathbf{H}_{\text{eff}} + \mathbf{H}_{\text{st}}) + \frac{\alpha}{M} \mathbf{M} \times \frac{\partial \mathbf{M}}{\partial t}, \quad (15)$$

where \mathbf{H}_{st} denotes the effective field from the SOT in Eq. (1),

$$\mathbf{H}_{\text{st}} = \frac{a}{M} \mathbf{M} \times \mathbf{J}_s - \beta a \mathbf{J}_s. \quad (16)$$

Because the spin current \mathbf{J}_s contains only one rf component, up to the linear term in the precessing magnetization \mathbf{m} , \mathbf{H}_{st} can be written as

$$\mathbf{H}_{\text{st}} = \text{Re}(\mathbf{h}_{\text{st}} e^{-i\omega t}), \quad (17)$$

where

$$\begin{aligned} \mathbf{h}_{\text{st}} &= -\frac{a}{M} \theta_{\text{SH}} \sigma_{\text{HM}} \left(\frac{\hbar}{2e}\right) \mathbf{M}_0 \times (\hat{z} \times \mathbf{e}) \\ &\quad + \beta a \theta_{\text{SH}} \sigma_{\text{HM}} \left(\frac{\hbar}{2e}\right) \hat{z} \times \mathbf{e}. \end{aligned} \quad (18)$$

Thus one can view st-FMR as the usual FMR under a total effective rf field of $\mathbf{h} + \mathbf{h}_{\text{st}}$, and the response of \mathbf{m} is

$$\mathbf{m} = \vec{\chi}(\mathbf{h} + \mathbf{h}_{\text{st}}) = \vec{\chi}\mathbf{h} + \vec{\kappa}\mathbf{e}. \quad (19)$$

\vec{k} relates to $\vec{\chi}$ as

$$\vec{k} = \vec{\chi} \left[-\frac{1}{M} \Lambda(\mathbf{M}_0) + \beta \right] a\theta_{\text{SH}} \sigma_{\text{HM}} \left(\frac{\hbar}{2e} \right) \Lambda(\hat{z}), \quad (20)$$

where Λ denotes the operator of cross product, i.e., $\Lambda(\mathbf{a})\mathbf{b} = \mathbf{a} \times \mathbf{b}$. Substituting the universal form of $\vec{\chi}(\omega)$ into Eq. (20),

one can obtain the universal form of frequency dependence of \vec{k} ,

$$\vec{k}(\omega) = a\theta_{\text{SH}} \sigma_{\text{HM}} \left(\frac{\hbar}{2e} \right) \frac{\pi\Gamma}{2} [L(\omega, \omega_0, \Gamma) + iD(\omega, \omega_0, \Gamma)] \vec{C}_e, \quad (21)$$

where

$$\vec{C}_e = \begin{pmatrix} [\beta C_3 + i(C_1 + \beta C_2)] \cos \theta & [C_3 + i(C_2 - \beta C_1)] \cos \theta & [\beta C_3 + i(C_1 + \beta C_2)] \sin \theta \\ [-C_3 + i(C_2 + \beta C_4)] \cos \theta & [\beta C_3 + i(C_4 - \beta C_2)] \cos \theta & [-C_3 + i(C_2 + \beta C_4)] \sin \theta \\ 0 & 0 & 0 \end{pmatrix}, \quad (22)$$

with θ being the polar angle of \mathbf{M}_0 in the xyz coordinate.

The field dependence of \vec{k} can be obtained by substituting Eq. (14) into Eq. (20),

$$\vec{k}(H) = a\theta_{\text{SH}} \sigma_{\text{HM}} \left(\frac{\hbar}{2e} \right) \frac{\pi\Gamma_1}{2} [L(H, H_0, \Gamma_1) - i\frac{\zeta}{|\zeta|} D(H, H_0, \Gamma_1)] \vec{C}_e. \quad (23)$$

Consequently, the magnetization motion at st-FMR can be expressed as

$$\begin{pmatrix} m_x \\ m_y \\ m_z \end{pmatrix} = \begin{pmatrix} \chi_{XX} & \chi_{XY} & 0 \\ \chi_{YX} & \chi_{YY} & 0 \\ 0 & 0 & 0 \end{pmatrix} \begin{pmatrix} h_x \\ h_y \\ h_z \end{pmatrix} + \begin{pmatrix} \kappa_{XX} & \kappa_{XY} & \kappa_{XZ} \\ \kappa_{YX} & \kappa_{YY} & \kappa_{YZ} \\ 0 & 0 & 0 \end{pmatrix} \begin{pmatrix} e_x \\ e_y \\ e_z \end{pmatrix}. \quad (24)$$

After the universal forms of $\vec{\chi}$ and \vec{k} are obtained, one is able to find the dc voltage signals attributed from the AMR, AHE, and ISHE.

C. The line shape of dc voltage

Substituting Eq. (24) into Eqs. (4), (5), and (9), U_{AMR} , U_{AHE} , and U_{ISHE} in terms of $\vec{\chi}$ and \vec{k} are

$$U_{\text{AMR}} = \frac{\Delta\rho}{2M} \text{Re}[(j_{\text{FM},i}^* l_z + j_{\text{FM},z}^* l_i)(\chi_{ij} h_j + \kappa_{ij} e_j)], \quad (25)$$

$$U_{\text{AHE}} = -\frac{R_1}{2} \text{Re}[\epsilon_{ijk} j_{\text{FM},j}^* l_i (\chi_{kl} h_l + \kappa_{kl} e_l)], \quad (26)$$

$$U_{\text{ISHE}} = -\frac{g_{\text{eff}}^{\downarrow} \theta_{\text{SHE}} \omega_Y \sin \theta}{2\pi \sigma_{\text{HM}} M^2} \text{Im}[(\chi_{X_i}^* h_i^* + \kappa_{X_i}^* e_i^*) \times (\chi_{Y_j} h_j + \kappa_{Y_j} e_j)], \quad (27)$$

where subscript indices i , j , k , and l can be X , Y , and Z . ϵ_{ijk} is the Levi-Civita symbol, and the Einstein summation convention is used. Whether a matrix element of $\vec{\chi}$ or \vec{k} is involved in dc voltage depends on the applied microwave fields and experimental setup. Substituting Eqs. (10), (13), (21), and (22) into Eqs. (25)–(27), the frequency dependence of dc voltage can be expressed in terms of Lorentzian and D functions,

$$U_{\text{AMR}}(\omega) = A_1 \frac{\pi\Gamma}{2} L(\omega, \omega_0, \Gamma) + A_2 \frac{\pi\Gamma}{2} D(\omega, \omega_0, \Gamma), \quad (28)$$

$$U_{\text{AHE}}(\omega) = A_3 \frac{\pi\Gamma}{2} L(\omega, \omega_0, \Gamma) + A_4 \frac{\pi\Gamma}{2} D(\omega, \omega_0, \Gamma), \quad (29)$$

$$U_{\text{ISHE}}(\omega) = A_5 \frac{\pi\Gamma}{2} L(\omega, \omega_0, \Gamma). \quad (30)$$

$A_1 \sim A_5$ are

$$A_1 = \frac{\Delta\rho}{2M} \text{Re} \left[(j_{\text{FM},i}^* l_z + j_{\text{FM},z}^* l_i) \left(C_{ij} h_j + \frac{\hbar}{2e} a\theta_{\text{SH}} C_{e,ij} j_{\text{HM},j} \right) \right],$$

$$A_2 = -\frac{\Delta\rho}{2M} \text{Im} \left[(j_{\text{FM},i}^* l_z + j_{\text{FM},z}^* l_i) \left(C_{ij} h_j + \frac{\hbar}{2e} a\theta_{\text{SH}} C_{e,ij} j_{\text{HM},j} \right) \right],$$

$$A_3 = -\frac{R_1}{2} \text{Re} \left[\epsilon_{ijk} j_{\text{FM},j}^* l_i \left(C_{kl} h_l + \frac{\hbar}{2e} a\theta_{\text{SH}} C_{e,kl} j_{\text{HM},l} \right) \right], \quad (31)$$

$$A_4 = \frac{R_1}{2} \text{Im} \left[\epsilon_{ijk} j_{\text{FM},j}^* l_i \left(C_{kl} h_l + \frac{\hbar}{2e} a\theta_{\text{SH}} C_{e,kl} j_{\text{HM},l} \right) \right],$$

$$A_5 = -\frac{g_{\text{eff}}^{\downarrow} \theta_{\text{SHE}} \omega_Y \sin \theta}{2\pi \sigma_{\text{HM}} M^2} \text{Im} \left[\left(C_{X_i}^* h_i^* + \frac{\hbar}{2e} a\theta_{\text{SH}} C_{e,X_i}^* j_{\text{HM},i} \right) \times \left(C_{Y_j} h_j + \frac{\hbar}{2e} a\theta_{\text{SH}} C_{e,Y_j} j_{\text{HM},j} \right) \right],$$

where subscript indices i , j , k , and l are x , y , and z . C_{ij} (or $C_{e,ij}$) is the element of the i th row and the j th column of matrix \vec{C} defined in Eq. (13) (or matrix \vec{C}_e defined in Eq. (22)). Starting from the universal forms of $\vec{\chi}(H)$ and $\vec{k}(H)$, one can also find the field dependence of dc-voltage line shapes,

$$U_{\text{AMR}}(H) = A_1 \frac{\pi\Gamma}{2} L(H, H_0, \Gamma_1) - \frac{\zeta}{|\zeta|} A_2 \frac{\pi\Gamma}{2} D(H, H_0, \Gamma_1), \quad (32)$$

$$U_{\text{AHE}}(H) = A_3 \frac{\pi\Gamma}{2} L(H, H_0, \Gamma_1) - \frac{\zeta}{|\zeta|} A_4 \frac{\pi\Gamma}{2} D(H, H_0, \Gamma_1), \quad (33)$$

$$U_{\text{ISHE}}(H) = A_5 \frac{\pi\Gamma}{2} L(H, H_0, \Gamma_1). \quad (34)$$

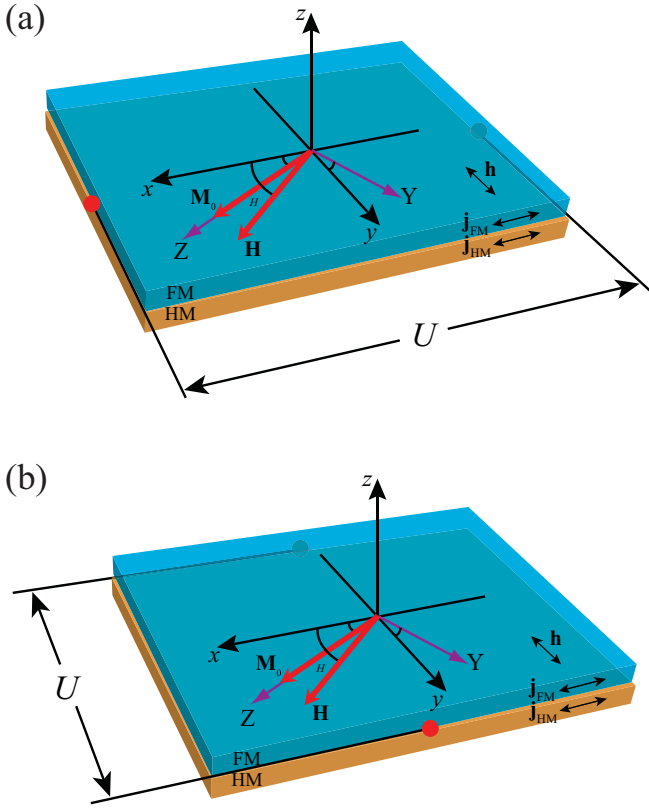


FIG. 2. Schematic illustration for two experimental configurations of st-FMR. A HM/FM bilayer lies in the xy plane. The stable magnetization \mathbf{M}_0 is in the sample plane by applying an in-plane static magnetic field \mathbf{H} . ϕ is the angle between \mathbf{M}_0 and the x axis, and ϕ_H is the angle between \mathbf{H} and the x axis. The definitions of the xyz and XYZ coordinates are the same as Fig. 1 with $\theta = 90^\circ$. The rf electric currents \mathbf{j}_{FM} and \mathbf{j}_{HM} are along the x -direction, and the rf Oersted field \mathbf{h} is along the y direction according to the Ampere's law. The displacement vector between two electrodes is along (a) the x or (b) the y directions.

The results tell us that the general dc-voltage line shape near the st-FMR have a *symmetric component* of the Lorentzian function and an *antisymmetric component* of the D function. $A_1 \sim A_5$ are linear combinations of $C_1 \sim C_4$ whose coefficients depend on magnetic anisotropy and experimental setup, and their values determine the relative weights of the symmetric and antisymmetric components.

III. RESULTS AND DISCUSSION

In this section, we use both easy-plane and biaxial models in two experimental configurations to illustrate possible angular dependence of dc voltage and dc-voltage line shape. We will also propose a proper way to experimentally determine spin-Hall angle of the HM.

Our model system, which mimics popular experimental setups, is shown in Fig. 2. A HM/FM bilayer film lies in the xy plane with the length l_x along the x direction and width l_y along the y direction. The rf current \mathbf{j}_a ($a = \text{FM, HM}$) is along the x axis. The effective magnetic field is

$$\mathbf{H}_{\text{eff}} = \mathbf{H} + K_x M_x \hat{x} - M_z \hat{z} + \text{Re}(\mathbf{h} e^{-i\omega t}), \quad (35)$$

where the static in-plane magnetic field \mathbf{H} is with a ϕ_H angle about the x axis, the second and third terms are, respectively, the easy axis and hard axis (shape) anisotropy fields, and the forth term is the rf Oersted field. In the following analyzes of two experimental configurations, we consider first easy-plane case of $K_x = 0$, and then the biaxial case of $K_x > 0$.

A. Dc-voltage along the rf current

In this configuration as shown in Fig. 2(a), the dc voltage is measured along the direction of rf electric current, i.e., $\mathbf{l} = l_x \hat{x}$. The dc voltage near the FMR comes from the AMR and ISHE because the dc electric field from AHE is transverse to the rf current. According to the spin pumping and ISHE, the dc current $\langle \mathbf{J}_{\text{ISHE}} \rangle$ near the FMR is in the sample plane and orthogonal to \mathbf{M}_0 . On the other hand, there is no magnetization precession and no spin pumping when \mathbf{M}_0 is along the \hat{y} direction because both Oersted field and SOT exert no torque on the magnetization. Thus $\langle \mathbf{J}_{\text{ISHE}} \rangle$ has a x component and results in a dc voltage along \hat{x} only when \mathbf{M}_0 deviates from the x and y directions.

1. Easy-plane case

For an easy-plane FM film where the z axis is the hard axis of the film, the stable magnetization \mathbf{M}_0 in the absence of microwave field is collinear with \mathbf{H} , i.e., $\phi = \phi_H$. According to Eq. (2), the linearized LLG equation in the present case becomes

$$-i\omega \mathbf{m} = -\gamma \mathbf{m} \times \mathbf{H} - \gamma \mathbf{M}_0 \times (\mathbf{h} - m_z \hat{z}), \quad -i\omega \frac{\alpha}{M} \mathbf{M}_0 \times \mathbf{m} + \gamma \frac{a}{M} \left(\frac{\hbar}{2e} \right) \theta_{\text{SH}} \sigma_{\text{HM}} \mathbf{M}_0 \times [\mathbf{M}_0 \times (\hat{z} \times \mathbf{e})], \quad (36)$$

where we assume that the fieldlike torque is very small and can be neglected, i.e., $\beta = 0$. The exact solution of this equation allows us to obtain the expressions of H_0 , Γ_1 , C_1 , C_2 , C_3 and C_4 which determine $\tilde{\chi}$ and $\tilde{\kappa}$ for an easy-plane model.

In the absence of any driving force and damping, from Eq. (36) it is easy to find the FMR frequency $\omega_0 = \gamma \sqrt{H(M+H)}$ which is the well-known Kittel's formula. Thus the resonance field H_0 for a given microwave frequency ω can be obtained as

$$H_0 = \sqrt{\frac{\omega^2}{\gamma^2} + \frac{M^2}{4}} - \frac{M}{2}. \quad (37)$$

To find the linewidth Γ_1 and the real numbers $C_1 \sim C_4$, we start from the nonzero matrix elements of $\tilde{\chi}$:

$$\begin{aligned} \chi_{XX} &= \frac{\gamma M (-\gamma H + i\alpha\omega)}{\omega^2 - \omega_0^2 + i\alpha\gamma\omega(M+2H)}, \\ \chi_{XY} &= -\chi_{YX} = \frac{i\omega\gamma M}{\omega^2 - \omega_0^2 + i\alpha\gamma\omega(M_s + 2H)}, \\ \chi_{YX} &= \frac{\gamma M (-\gamma H - \gamma M + i\alpha\omega)}{\omega^2 - \omega_0^2 + i\alpha\gamma\omega(M+2H)}. \end{aligned} \quad (38)$$

Equation (38) can be written as the sum of a Lorentzian function and an D function near the resonance field H_0 . In terms of parameters defined in Eq. (21)–(23), it is easy to

obtain

$$\Gamma_1 = \frac{2\alpha\omega}{\gamma}, \quad (39)$$

and

$$\begin{aligned} C_1 &= \frac{\gamma M H_0}{\alpha\omega(2H_0 + M)}, \\ C_2 &= 0, \\ C_3 &= \frac{M}{\alpha(2H_0 + M)}, \\ C_4 &= \frac{\gamma M(H_0 + M)}{\alpha\omega(2H_0 + M)}, \end{aligned} \quad (40)$$

where Eq. (39) is usually used in experiments to determine the Gilbert damping coefficient α . From the Kittel's formula, it is obvious that $\zeta > 0$ which results in a minus sign in front of D function in Eqs. (14), (32), and (33). It is only true for an easy-plane model in which H_0 , Γ_1 , and $C_1 \sim C_4$ does not depend on ϕ_H for an in-plane field \mathbf{H} . For a biaxial model where $K_x > 0$, all these parameters depend on ϕ_H in general.

In the XYZ coordinate, the displacement $\mathbf{l} = l_x \hat{x}$ between the two electrodes becomes

$$\mathbf{l} = -l_x \sin \phi \hat{Y} + l_x \cos \phi \hat{Z}. \quad (41)$$

The dc voltage from each contribution can be obtained by substituting Eqs. (37)–(40) and Eq. (41) into Eq. (31),

$$\begin{aligned} A_1 &= \frac{\Delta\rho j_{\text{HM}} j_{\text{FM}} l_x}{2\alpha(2H_0 + M)} a\theta_{\text{SH}} \frac{\hbar}{2e} \sin 2\phi_H \cos \phi_H, \\ A_2 &= \frac{\Delta\rho j_{\text{HM}} j_{\text{FM}} l_x \omega}{2\alpha\gamma H_0(2H_0 + M)} \frac{d_{\text{HM}}}{2} \sin 2\phi_H \cos \phi_H, \\ A_3 &= A_4 = 0, \\ A_5 &= \frac{g_{\text{eff}}^{\uparrow\downarrow} \theta_{\text{SH}} e j_{\text{HM}}^2 l_x \gamma H_0}{4\pi\alpha^2 \sigma_{\text{HM}} (2H_0 + M)^2} \left[\left(a\theta_{\text{SH}} \frac{\hbar}{2e} \right)^2 + \left(\frac{\omega d_{\text{HM}}}{2\gamma H_0} \right)^2 \right] \\ &\quad \times \sin 2\phi_H \cos \phi_H. \end{aligned} \quad (42)$$

A_1 and A_2 are, respectively, from the AMR contribution due to the rf SOT driven and rf Oersted field driven magnetization motion. Thus A_1 is proportional to \mathbf{j}_s converted from \mathbf{j}_{HM} via SHE that, in turn, is proportional to θ_{SH} , while A_2 is independent of θ_{SH} . Both A_3 and A_4 are zero due to the absence of the AHE contribution as mentioned before. The two terms in A_5 depend on θ_{SH} . One is linear in θ_{SH} because of ISHE. The other is proportional to its cubic form. This is because the spin current is proportional to the square of amplitude of magnetization deviation that, in turn, come from both rf Oersted field that does not depends on θ_{SH} and the effective field generated by rf SOT that is proportional to θ_{SH} due to SHE.

Equation (42) indicates that both symmetric and anti-symmetric components of dc-voltage line shapes follow the same angular dependence of $\sin 2\phi_H \cos \phi_H$. In the previous estimation of the spin-Hall angle θ_{SH} , U_{ISHE} is assumed to be negligible, i.e., $A_5 = 0$, for the reason that U_{ISHE} is high order in the spin-Hall angle [21]. Thus the symmetric component of dc voltage signal is completely from the AMR. Under this assumption, the spin-Hall angle can be estimated by

$\theta_{\text{SH}} = \frac{S}{A} \frac{\omega d_{\text{HME}}}{\alpha\gamma H_0 \hbar}$, where S and A are, respectively, the amplitudes of symmetric and antisymmetric components of dc-voltage line shape for any angle ϕ_H . However, the estimated value by this approach is found to be overestimated compared with spin pumping experiments [20,26,28,29], which indicates that this assumption is questionable.

A more precise estimation of the spin-Hall angle θ_{SH} can be obtained by taking into account the ISHE contribution of dc voltage. According to Eq. (42), U_{ISHE} has the exact same symmetry and angular dependence as the AMR contribution to dc voltage due to SOT, however, it will not prevent one from obtaining θ_{SH} . Starting from Eq. (42), the ratio S/A , where $S = A_1 + A_3 + A_5$ and $A = A_2 + A_4$, is

$$\frac{S}{A} = a_1 \theta_{\text{SH}} + a_2 \theta_{\text{SH}}^3, \quad (43)$$

where S/A is measured in experiments, and a_1 and a_2 are

$$\begin{aligned} a_1 &= \frac{\alpha\gamma H_0 \hbar}{\omega d_{\text{HME}}} + \frac{g_{\text{eff}}^{\uparrow\downarrow} e \omega d_{\text{HM}}}{4\pi\alpha(2H_0 + M)\Delta\rho\sigma_{\text{FM}}}, \\ a_2 &= \frac{a^2 g_{\text{eff}}^{\uparrow\downarrow} \gamma^2 H_0^2 \hbar^2}{4\pi\alpha(2H_0 + M)\Delta\rho\sigma_{\text{FM}}\omega d_{\text{HME}}}. \end{aligned} \quad (44)$$

Consequently, the corrected value of θ_{SH} can be determined from Eq. (43) since θ_{SH} is the only unknown. Different from the previous argument [21], two terms on the right-hand side of Eq. (43) are in general of the same order for typical materials so that θ_{SH} is not proportional to the ratio S/A as claimed before.

Figure 3 shows the comparison between the dc-voltage line shapes of the current theory (solid curves) and the experimental results of Refs. [21] (a), [22] (b), [23] (c), and [24] (d) (squares) that used the experimental setup discussed in this section. For Fig. 3(a), the red and green squares are extracted from the experimental results for Pt(6)/Py(4) and Pt(15)/Py(15), respectively, while the red and green solid curves are the best fittings of the current theory with $\theta_{\text{SH}} = 0.05$ and following material parameters of $\Delta\rho\sigma_{\text{FM}} = 2\%$, $g_{\text{eff}}^{\uparrow\downarrow} = 3.02 \times 10^{19} \text{ m}^{-2}$, $M = 6.4 \times 10^5 \text{ A/m}$ for Pt(6)/Py(4) [or $M = 8.34 \times 10^5 \text{ A/m}$ for Pt(15)/Py(15)] and $\alpha = 0.028$ for Pt(6)/Py(4) [or $\alpha = 0.0123$ for Pt(15)/Py(15)] [21] [some of the parameters are extracted from experimental curves of H_0 and Γ_1 by using the Kittel's formula and Eq. (39)]. Because j_{HM} and j_{FM} are unknown and change only the absolute values of dc voltage without affecting the spin-Hall angle, we use $\Delta\rho j_{\text{HM}} j_{\text{FM}} l_x = 1.536 \times 10^8 \text{ V A m}^{-2}$ for Pt(6)/Py(4) and $\Delta\rho j_{\text{HM}} j_{\text{FM}} l_x = 7.862 \times 10^7 \text{ V A m}^{-2}$ for Pt(15)/Py(15) in the fitting. The theoretical curves in Fig. 3(a) agree well with the experimental results of Ref. [21] with the same spin-Hall angle $\theta_{\text{SH}} = 0.05$, in contrast to very different θ_{SH} values for Pt with different thickness [21] that is in conflict with the belief of spin-Hall angle as an intrinsic material parameter. For Fig. 3(b), the squares are extracted from the experimental results for Pt(6)/Py(5.5), while the solid curves are the best fittings of the current theory with $\theta_{\text{SH}} = 0.045$ and following material parameters of $g_{\text{eff}}^{\uparrow\downarrow} = 3.96 \times 10^{19} \text{ m}^{-2}$, $M = 7.5 \times 10^5 \text{ A/m}$, and $\alpha = 0.016$. The theoretical curves in Fig. 3(b) agree well with the experimental results of Ref. [22] with the spin-Hall angle $\theta_{\text{SH}} = 0.045$,

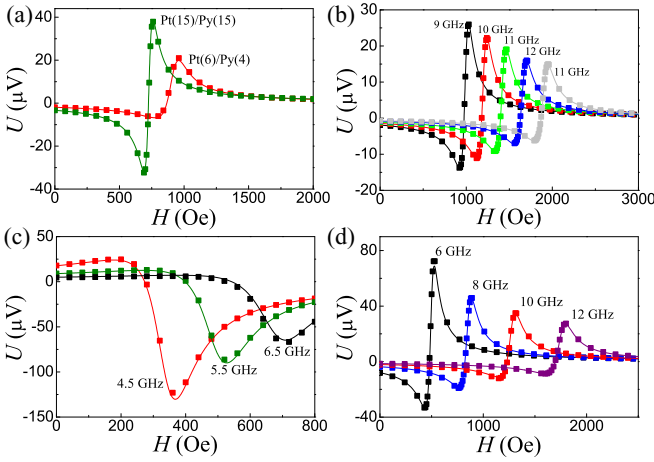


FIG. 3. Comparison between the current theory (solid curves) and experimental results (squares). (a) The fitting of data from Ref. [21] for Pt(6)/Py(4) (red) and Pt(15)/Py(15) (green), respectively. The Pt/Py parameters are $M = 6.4 \times 10^5$ A/m for Pt(6)/Py(4) [or $M = 8.34 \times 10^5$ A/m for Pt(15)/Py(15)], $\alpha = 0.028$ for Pt(6)/Py(4) [or $\alpha = 0.0123$ for Pt(15)/Py(15)], $\Delta\rho\sigma_{\text{FM}} = 2\%$, $g_{\text{eff}}^{\uparrow\downarrow} = 3.02 \times 10^{19} \text{ m}^{-2}$, and $\theta_{\text{SH}} = 0.05$. $\Delta\rho j_{\text{HM}} j_{\text{FM}} l_x = 1.536 \times 10^8 \text{ V A m}^{-2}$ for Pt(6)/Py(4) and $\Delta\rho j_{\text{HM}} j_{\text{FM}} l_x = 7.862 \times 10^7 \text{ V A m}^{-2}$ for Pt(15)/Py(15) are used for the fittings. (b) The fitting of data from Ref. [22] for Pt(6)/Py(5.5). The Pt/Py parameters are $g_{\text{eff}}^{\uparrow\downarrow} = 3.96 \times 10^{19} \text{ m}^{-2}$, $M = 7.5 \times 10^5$ A/m, $\alpha = 0.016$, and $\theta_{\text{SH}} = 0.045$. (c) The fitting of data from Ref. [23] for Pt(4)/Py(2.5). The Pt/Py parameters are $g_{\text{eff}}^{\uparrow\downarrow} = 3.02 \times 10^{19} \text{ m}^{-2}$, $M = 5.8 \times 10^5$ A/m, $\alpha = 0.043$, and $\theta_{\text{SH}} = 0.05$. (d) The fitting of data from Ref. [24] for Pt(6)/Py(5). The Pt/Py parameters are $g_{\text{eff}}^{\uparrow\downarrow} = 3.02 \times 10^{19} \text{ m}^{-2}$, $M = 6.97 \times 10^5$ A/m, $\alpha = 0.02$, and $\theta_{\text{SH}} = 0.061$.

which is much smaller than 0.19 obtained in Ref. [22]. For Fig. 3(c), the squares are extracted from the experimental results for Py(2.5)/Pt(4), while the solid curves are the best fittings of the current theory with $\theta_{\text{SH}} = 0.05$ and following material parameters of $g_{\text{eff}}^{\uparrow\downarrow} = 3.02 \times 10^{19} \text{ m}^{-2}$, $M = 5.8 \times 10^5$ A/m and $\alpha = 0.043$. The theoretical curves in Fig. 3(c) agree again well with the experimental results of Ref. [23] with the spin-Hall angle $\theta_{\text{SH}} = 0.05$ which is smaller than 0.087 obtained in Ref. [23]. For Fig. 3(d), the squares are extracted from the experimental results for Py(5)/Pt(6), while the solid curves are the best fittings of the current theory with $\theta_{\text{SH}} = 0.061$ and following material parameters of $g_{\text{eff}}^{\uparrow\downarrow} = 3.02 \times 10^{19} \text{ m}^{-2}$, $M = 6.97 \times 10^5$ A/m, and $\alpha = 0.02$. The theoretical curves in Fig. 3(d) agree well with the experimental results of Ref. [24] with the spin-Hall angle $\theta_{\text{SH}} = 0.061$ which is smaller than 0.068 obtained in Ref. [24]. Our results indicate that the spin-Hall angle can be overestimated in st-FMR without considering the effect of spin pumping and ISHE.

2. Biaxial case

For a general biaxial case with the easy axis anisotropy coefficient $K_x > 0$, the static magnetization \mathbf{M}_0 in the absence of microwave fields is noncollinear to static magnetic field \mathbf{H} , i.e., $\phi \neq \phi_H$ but $\phi = \phi(\phi_H)$.

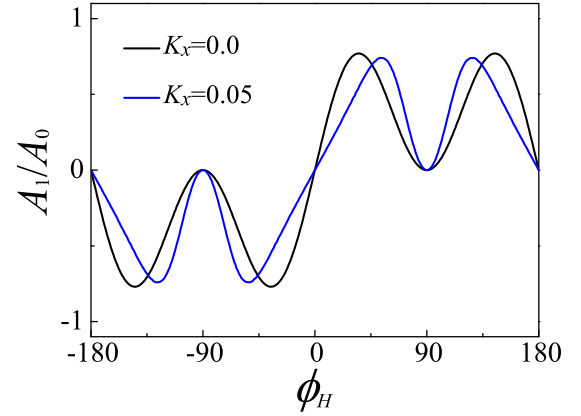


FIG. 4. Angular dependence of A_1 in units of $A_0 = \frac{\Delta\rho j_{\text{HM}} j_{\text{FM}} l_x a \theta_{\text{SH}}}{2\alpha(2H_0+M)} \frac{\hbar}{2e}$ for the setup shown in Fig. 2(a). The model parameters are $\omega = 2\pi \times 9.0$ GHz, $M = 8.0 \times 10^5$ A/m, and easy axis anisotropy coefficient $K_x = 0.0$ (black curve) or $K_x = 0.05$ (blue curve). The black curve is plotted according to Eq. (42), and the blue curve is numerically calculated from Eq. (45).

$H_0(\phi_H)$, $\Gamma_1(\phi_H)$, $C_1(\phi_H)$, $C_3(\phi_H)$, and $C_4(\phi_H)$ are all functions of ϕ_H , which can be numerically obtained once the material parameters are given or be determined by standard microwave absorption measurements [35]. Notice that $C_2 = 0$ is still satisfied because the energy density function corresponding to the effective field of Eq. (35) is symmetric about the YZ plane (or the xy plane) [35]. Consequently, from Eq. (31), one can obtain the dc voltage for a biaxial model as follows:

$$\begin{aligned} A_1 &= a_{\text{AMR}} C_3(\phi_H) \sin 2\phi(\phi_H) \cos \phi(\phi_H), \\ A_2 &= b_{\text{AMR}} C_4(\phi_H) \sin 2\phi(\phi_H) \cos \phi(\phi_H), \\ A_3 &= A_4 = 0, \\ A_5 &= [a_{\text{ISHE},1} C_1(\phi_H) + a_{\text{ISHE},2} C_4(\phi_H)] \\ &\quad \times C_3(\phi_H) \sin 2\phi(\phi_H) \cos \phi(\phi_H), \end{aligned} \quad (45)$$

where

$$\begin{aligned} a_{\text{AMR}} &= \frac{\Delta\rho j_{\text{HM}} j_{\text{FM}} l_x}{2M} a \theta_{\text{SH}} \frac{\hbar}{2e}, \\ b_{\text{AMR}} &= \frac{\Delta\rho j_{\text{HM}} j_{\text{FM}} l_x}{2M} \frac{d_{\text{HM}}}{2}, \\ a_{\text{ISHE},1} &= \frac{g_{\text{eff}}^{\uparrow\downarrow} \theta_{\text{SH}} e \omega j_{\text{HM}}^2 l_x}{4\pi \sigma_{\text{HM}} M^2} \left(a \theta_{\text{SH}} \frac{\hbar}{2e} \right)^2, \\ a_{\text{ISHE},2} &= \frac{g_{\text{eff}}^{\uparrow\downarrow} \theta_{\text{SH}} e \omega j_{\text{HM}}^2 l_x}{4\pi \sigma_{\text{HM}} M^2} \left(\frac{d_{\text{HM}}}{2} \right)^2. \end{aligned} \quad (46)$$

Obviously, the angular dependence of dc voltage in a biaxial model no longer follows $\sin 2\phi_H \cos \phi_H$. The angular dependences of different components are different in a biaxial model because A_1 and A_2 are respectively proportional to $C_3(\phi_H)$ and $C_4(\phi_H)$, and A_5 is proportional to linear combinations of $C_1(\phi_H)C_3(\phi_H)$ and $C_3(\phi_H)C_4(\phi_H)$. This allows one to separate various contributions to dc voltage. Figure 4 shows the angular dependence of A_1 for an easy-plane ($K_x = 0$) model (black curve) and a biaxial model of $K_x = 0.05$ (blue curve)

for $\omega = 2\pi \times 9.0$ GHz and $M = 8.0 \times 10^5$ A/m. The black and blue curves are, respective, plots of Eq. (42) and Eq. (45). For both cases, A_1 is in the units of $A_0 = \frac{\Delta\rho j_{\text{HM}} j_{\text{FM}} l_y a_{\text{SH}}}{2\alpha(2H_0 + M)} \frac{\hbar}{2e}$. The angular dependence of A_1 for an easy-plane model follows $\sin 2\phi_H \cos \phi_H$, while, for a biaxial model of $K_x = 0.05$, it apparently deviates from $\sin 2\phi_H \cos \phi_H$. Thus one can tell whether or not an FM is a biaxial magnetic film by looking at the angular dependence of dc voltage.

From Eqs. (45) and (46), following recipe can be used to determine the spin-Hall angle. *Step I.* Determine the angular dependence of C_i ($i = 1, 2, 3, 4$) by standard microwave absorption experiments [35]. *Step II.* After $C_i(\phi_H)$ ($i = 1, 2, 3, 4$) is obtained, determine a_{AMR} , b_{AMR} , $a_{\text{ISHE},1}$ and $a_{\text{ISHE},2}$ by fitting the experimental curves according to Eq. (45). *Step III.* The spin-Hall angle θ_{SH} can be determined by

$$\theta_{\text{SH}} = \frac{d_{\text{HM}} e a_{\text{AMR}}}{a \hbar b_{\text{AMR}}}. \quad (47)$$

From the above steps, the spin-Hall angle can be determined for a biaxial sample in the experimental setup of Fig. 2(a).

B. Direct-current-voltage transverse to the rf current

Figure 2(b) is another useful experimental configuration in which the dc voltage is measured transverse to rf current direction. Different from the configuration in Fig. 2(a), AMR, AHE and ISHE will all contribute to dc voltage in this case. Since the AHE generates a dc electric field transverse to rf current, it should be very important in the present configuration. As mentioned before that $\langle \mathbf{J}_{\text{ISHE}} \rangle$ is in the sample plane and orthogonal to \mathbf{M}_0 , $\langle \mathbf{J}_{\text{ISHE}} \rangle$ has in general a y component and can result in a dc voltage along \hat{y} when \mathbf{M}_0 is not parallel to \hat{y} .

1. Easy-plane case

For an easy-plane model, H_0 , Γ_1 , and $C_1 \sim C_4$ are given by Eqs. (37)–(40). In the XYZ coordinate, the displacement $\mathbf{l} = l_y \hat{y}$ is

$$\mathbf{l} = l_y \cos \phi \hat{Y} + l_y \sin \phi \hat{Z}. \quad (48)$$

Substituting Eqs. (37)–(40) and Eq. (48) into Eq. (31), the amplitude of each dc voltage component is

$$\begin{aligned} A_1 &= a_{\text{AMR}} \cos 2\phi_H \cos \phi_H, \\ A_2 &= b_{\text{AMR}} \cos 2\phi_H \cos \phi_H, \\ A_3 &= a_{\text{AHE}} \cos \phi_H, \\ A_4 &= b_{\text{AHE}} \cos \phi_H, \\ A_5 &= a_{\text{ISHE}} \cos^3 \phi_H, \end{aligned} \quad (49)$$

where

$$\begin{aligned} a_{\text{AMR}} &= -\frac{\Delta\rho j_{\text{HM}} j_{\text{FM}} l_y}{2\alpha(2H_0 + M)} a_{\text{SH}} \frac{\hbar}{2e}, \\ b_{\text{AMR}} &= -\frac{\Delta\rho j_{\text{HM}} j_{\text{FM}} l_y \omega}{2\alpha\gamma H_0(2H_0 + M)} \frac{d_{\text{HM}}}{2}, \\ a_{\text{AHE}} &= \frac{R_1 j_{\text{HM}} j_{\text{FM}} l_y M}{2\alpha(2H_0 + M)} \frac{d_{\text{HM}}}{2}, \end{aligned}$$

$$\begin{aligned} b_{\text{AHE}} &= -\frac{R_1 j_{\text{HM}} j_{\text{FM}} l_y \gamma M H_0}{2\alpha\omega(2H_0 + M)} a_{\text{SH}} \frac{\hbar}{2e}, \\ a_{\text{ISHE}} &= -\frac{g_{\text{eff}}^{\uparrow\downarrow} \theta_{\text{SH}} e j_{\text{HM}}^2 l_y \gamma H_0}{2\pi\alpha^2\sigma_{\text{HM}}(2H_0 + M)^2} \left[\left(a_{\text{SH}} \frac{\hbar}{2e} \right)^2 + \left(\frac{\omega d_{\text{HM}}}{2\gamma H_0} \right)^2 \right]. \end{aligned} \quad (50)$$

a_{AMR} and b_{AHE} are, respectively, from the AMR and AHE due to the rf SOT driven magnetization motion. Thus they are proportional to \mathbf{j}_s converted from \mathbf{j}_{HM} via SHE and is proportional to θ_{SH} . On the other hand, b_{AMR} and a_{AHE} are, respectively, from the AMR and AHE due to the rf Oersted field driven magnetization motion, so they are related to neither the SHE nor ISHE and are independent of θ_{SH} . a_{ISHE} has two terms which, are, respectively, proportional to θ_{SH}^3 and θ_{SH} for the similar reason mentioned below Eq. (42).

Different from the previous case, the angular dependence of dc voltages from the AMR, AHE and ISHE are not the same in the present configuration. The issue is then how to determine a_{AMR} , b_{AMR} , a_{AHE} , b_{AHE} , and a_{ISHE} to distinguish each contribution to dc voltage and find the spin-Hall angle θ_{SH} . The symmetric component contains three different angular dependencies: $\cos 2\phi \cos \phi$, $\cos \phi$, and $\cos^3 \phi$, however, these three functions are not linearly independent. Thus a symmetric curve cannot uniquely determine the coefficients, and we should start from the antisymmetric part where the angular dependences $\cos 2\phi \cos \phi$ and $\cos \phi$ are linearly independent with each other.

From Eqs. (49) and (50), following recipe can be used to distinguish each dc voltage contribution and determine the spin-Hall angle. *Step I.* Fit the angular dependence of antisymmetric component of dc voltage by $\cos 2\phi \cos \phi$ and $\cos \phi$. The fitting numbers of $\cos 2\phi \cos \phi$ and $\cos \phi$ are b_{AMR} and b_{AHE} , respectively. *Step II.* a_{AMR} and a_{AHE} can be determined by $a_{\text{AMR}} = \frac{\Delta\rho}{R_1} \frac{\omega}{\gamma M H_0} b_{\text{AHE}}$ and $a_{\text{AHE}} = -\frac{R_1}{\Delta\rho} \frac{\gamma M H_0}{\omega} b_{\text{AMR}}$. *Step III.* Subtracting a_{AMR} and a_{AHE} terms from the symmetric component of dc voltage, the rest part comes from ISHE and can determine a_{ISHE} using Eq. (49). *Step IV.* The spin-Hall angle can be determined by

$$\theta_{\text{SH}} = \frac{\omega d_{\text{HME}} a_{\text{AMR}}}{a\gamma H_0 \hbar b_{\text{AMR}}} = -\frac{\omega d_{\text{HME}} e b_{\text{AHE}}}{a\gamma H_0 \hbar a_{\text{AHE}}}. \quad (51)$$

From the above steps, the dc voltage from each source can be distinguished and the spin-Hall angle can be determined for an easy-plane sample in the setup of Fig. 2(b).

According to Eq. (50), one has

$$\frac{a_{\text{AMR}}}{b_{\text{AMR}}} = -\frac{b_{\text{AHE}}}{a_{\text{AHE}}}. \quad (52)$$

This measures the ratio of the rf SOT and the torque by rf Oersted field. If Eq. (52) cannot be satisfied after one extracts all numbers from an experiment, it may indicate additional effects beyond the current model, e.g., the extraordinary galvanomagnetic effects in polycrystalline magnetic films [50], or the longitudinal ISHE, which will be discussed in the next section.

2. Biaxial case

We consider a biaxial model in the configuration of Fig. 2(b). The model is the same as the biaxial model used in the configuration of Fig. 2(a) but replace $\mathbf{l} = l_x \hat{x}$ by $\mathbf{l} = l_y \hat{y}$. By applying the biaxial model into the universal forms of dynamic magnetic susceptibility and dc-voltage line shape, one can obtain

$$\begin{aligned} A_1 &= a_{\text{AMR}} C_3(\phi_H) \cos 2\phi(\phi_H) \cos \phi(\phi_H), \\ A_2 &= b_{\text{AMR}} C_4(\phi_H) \cos 2\phi(\phi_H) \cos \phi(\phi_H), \\ A_3 &= a_{\text{AHE}} C_3(\phi_H) \cos \phi(\phi_H), \\ A_4 &= b_{\text{AHE}} C_1(\phi_H) \cos \phi(\phi_H), \\ A_5 &= [a_{\text{ISHE},1} C_1(\phi_H) + a_{\text{ISHE},2} C_4(\phi_H)] \\ &\quad \times C_3(\phi_H) \cos^3 \phi(\phi_H), \end{aligned} \quad (53)$$

where

$$\begin{aligned} a_{\text{AMR}} &= -\frac{\Delta\rho j_{\text{HM}} j_{\text{FM}} l_y}{2M} a\theta_{\text{SH}} \frac{\hbar}{2e}, \\ b_{\text{AMR}} &= -\frac{\Delta\rho j_{\text{HM}} j_{\text{FM}} l_y}{2M} \frac{d_{\text{HM}}}{2}, \\ a_{\text{AHE}} &= \frac{R_1 j_{\text{HM}} j_{\text{FM}} l_y}{2} \frac{d_{\text{HM}}}{2}, \\ b_{\text{AHE}} &= -\frac{R_1 j_{\text{HM}} j_{\text{FM}} l_y}{2} a\theta_{\text{SH}} \frac{\hbar}{2e}, \\ a_{\text{ISHE},1} &= -\frac{g_{\text{eff}}^{\uparrow\downarrow} \theta_{\text{SH}} e \omega j_{\text{HM}}^2 l_y}{2\pi \sigma_{\text{HM}} M^2} \left(a\theta_{\text{SH}} \frac{\hbar}{2e} \right)^2, \\ a_{\text{ISHE},2} &= -\frac{g_{\text{eff}}^{\uparrow\downarrow} \theta_{\text{SH}} e \omega j_{\text{HM}}^2 l_y}{2\pi \sigma_{\text{HM}} M^2} \left(\frac{d_{\text{HM}}}{2} \right)^2, \end{aligned} \quad (54)$$

from which it is obvious that the angular dependence differs from that of the easy-plane model. For the similar reasons mentioned after Eq. (50), a_{AMR} and b_{AHE} are proportional to θ_{SH} while b_{AMR} and a_{AHE} are independent of θ_{SH} . Two terms from the ISHE are characterized by $a_{\text{ISHE},1}$ and $a_{\text{ISHE},2}$.

From Eqs. (53) and (54), following recipe can be used to separate dc voltage signals from different contributions and to extract the spin-Hall angle.

Step I. Determine the angular dependence of C_i ($i = 1, 2, 3, 4$) by standard microwave absorption experiments [35]. *Step II.* After $C_i(\phi_H)$ ($i = 1, 2, 3, 4$) is obtained, determine a_{AMR} , b_{AMR} , a_{AHE} , b_{AHE} , $a_{\text{ISHE},1}$, and $a_{\text{ISHE},2}$ by fitting the experimental curves according to Eq. (53). *Step III.* The spin-Hall angle θ_{SH} can be still determined by Eq. (51). From the above steps, the dc voltage from each source can be distinguished and the spin-Hall angle can be determined for a biaxial sample in the experimental configuration of Fig. 2(b).

Again, one can use Eq. (52) to test the model. If the extract model parameters do not satisfy Eq. (52), then there may exist other sources for the dc voltage like the extraordinary galvanomagnetic effects [50], or the longitudinal ISHE discussed below.

C. Discussion

So far, the electric current density converted from a spin current of polarization \vec{p} and magnitude J^s flowing along the

z direction via the ISHE is assumed to be $\theta_{\text{SH}} J^s \hat{z} \times \vec{p}$. In magnetic materials, however, the general physics principle can allow other types of electric current density when spins, charges, orbits and magnetization interact with each. Let J_{ij}^s be the component of rank-2 spin current tensor \vec{J}^s with spin polarization along the j direction (\vec{p}) and flowing along the i direction (\hat{z} in the current case).

Similar to the derivation of AMR [50] under the assumption of physics law being coordinate independent, the most general charge current density \mathbf{J}^c of a vector converted from a spin current \vec{J}^s , within the linear response (to \vec{J}^s), should be

$$J_k^c = \frac{2e}{\hbar} \theta_{ijk}^{\text{SH}} J_{ij}^s,$$

where J_k^c is the charge current density along the k direction and θ_{ijk}^{SH} is the ijk component of the general spin-Hall angle tensor $\vec{\theta}^{\text{SH}}$ of rank 3 that depends on \mathbf{M} . $i, j, k = 1, 2, 3$ stands for $x, y,$ and z directions and the Einstein summation convention is assumed. The most general form of θ_{ijk}^{SH} is

$$\begin{aligned} \theta_{ijk}^{\text{SH}} &= \theta_0^{\text{SH}} \epsilon_{ijk} + \theta_1^{\text{SH}} M_l \epsilon_{iln} \epsilon_{jnk} \\ &\quad + \theta_2^{\text{SH}} M_l M_n \epsilon_{ilp} \epsilon_{j pq} \epsilon_{kqn} + \theta_3^{\text{SH}} M_i M_j M_k, \end{aligned} \quad (55)$$

where ϵ_{ijk} is the usual Levi-Civita symbol. $\theta_0^{\text{SH}} = \theta_{\text{SH}}$ is the usual spin-Hall angle that does not interact with \mathbf{M} , $\theta_\alpha^{\text{SH}}$ ($\alpha = 1, 2, 3$) that are, respectively, linear, quadratic, and cubic in \mathbf{M} . In the following, we limit ourselves to the first two terms, and discuss the generated charge current in two cases: (1) the spin current flows along its polarization \vec{p} and (2) the spin current flows transverse to its polarization \vec{p} .

Consider the first case where the spin current only has J_{33}^s component, we then have $\theta_{33k}^{\text{SH}} = \theta_1^{\text{SH}} M_l \epsilon_{3ln} \epsilon_{3nk}$, which results in two possible cases ($l = 1, n = 2, k = 1$) and ($l = 2, n = 1, k = 2$). Then we can obtain $J_1^c = -(\frac{2e}{\hbar}) \theta_1^{\text{SH}} M_1 J_{33}^s$ and $J_2^c = -(\frac{2e}{\hbar}) \theta_1^{\text{SH}} M_2 J_{33}^s$. It says that a charge current can be generated along the magnetization perpendicular to spin flowing direction (as well as the spin polarization), as shown in Fig. 5(a).

For the second case where the spin current only has J_{31}^s component, we have $\theta_{31k}^{\text{SH}} = \theta_{\text{SH}} \epsilon_{31k} + \theta_1^{\text{SH}} M_l \epsilon_{3ln} \epsilon_{1nk}$. The resulted charge current components are $J_2^c = (\frac{2e}{\hbar}) \theta_{\text{SH}} J_{31}^s$ and $J_3^c = (\frac{2e}{\hbar}) \theta_1^{\text{SH}} M_1 J_{31}^s$, where J_2^c is similar to the usual ISHE that the charge current is perpendicular to both spin polarization and spin flow direction, while J_3^c is a new term. It says that, due to the interaction between the spin current and magnetization, a charge current flows along the spin flowing direction when the magnetization is along the spin polarization direction, as shown in Fig. 5(b).

Similar to the generalized ISHE in a magnetic material, the SHE can also exist in a magnetic material. The most general linear response to \mathbf{J}^c in terms of possible spin current \vec{J}^s is

$$J_{ij}^s = \frac{\hbar}{2e} \theta_{ijk}^{\text{SH}} J_k^c,$$

where J_k^c is the charge current density along the k direction and θ_{ijk}^{SH} is the ijk component of the general spin-Hall angle tensor $\vec{\theta}^{\text{SH}}$ of rank 3 that depends on \mathbf{M} . $\vec{\theta}^{\text{SH}}$ is given by the same expression as that of Eq. (55). Without losing the

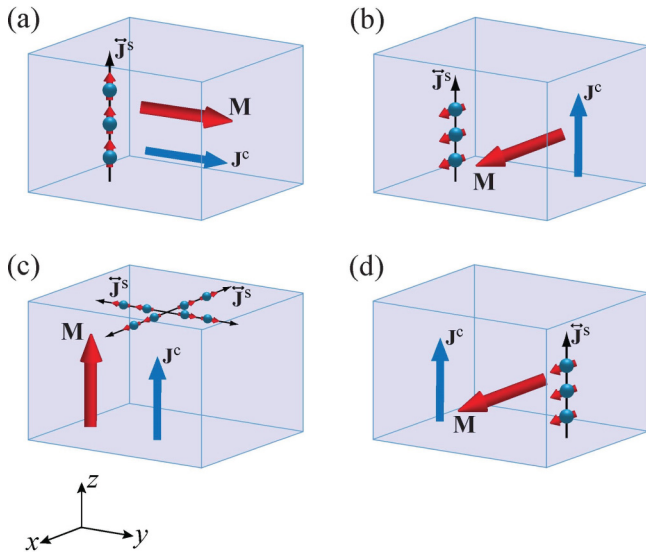


FIG. 5. Schematics of new ISHE [(a) and (b)] and SHE [(c) and (d)] in magnetic materials. (a) For a spin current flowing along the spin polarization direction, a charge current can be generated along the magnetization perpendicular to spin flowing direction (as well as the spin polarization). (b) For a spin current flowing perpendicular to the spin polarization direction, a charge current flows along the spin flowing direction when the magnetization is along the spin polarization direction. (c) For a charge current flowing along the magnetization, the generated spin current flows perpendicular to the charge current and the spin polarization is along the spin flow direction. (d) For a charge current flowing perpendicular to the magnetization, the generated spin current is along the charge current and the spin polarization is along the magnetization.

generality, we let charge current along the z direction. There are two possible cases: (1) the charge current flows along \mathbf{M} and (2) the charge current flows perpendicular to \mathbf{M} .

In the first case, we have $\theta_{ij3}^{\text{SH}} = \theta_{\text{SH}}\epsilon_{ij3} + \theta_1^{\text{SH}}M_3\epsilon_{i3n}\epsilon_{jn3}$. Up to the linear term in \mathbf{M} , the first term is the usual spin-Hall angle, and the new spin currents from the second term are $J_{11}^s = -(\frac{\hbar}{2e})\theta_1^{\text{SH}}M_3J_3^c$ and $J_{22}^s = -(\frac{\hbar}{2e})\theta_1^{\text{SH}}M_3J_3^c$. It says that, due to the interaction between the charge current and magnetization, the generated spin current flows perpendicular

to charge current and the spin polarization is along the spin flowing direction, as shown in Fig. 5(c).

In the second case, without losing the generality we let \mathbf{M} along the x direction. We then have $\theta_{ij3}^{\text{SH}} = \theta_{\text{SH}}\epsilon_{ij3} + \theta_1^{\text{SH}}M_1\epsilon_{i1n}\epsilon_{jn3}$. Up to the linear term in \mathbf{M} , the first term is the usual spin-Hall angle, and the new spin current from the second term is $J_{31}^s = (\frac{\hbar}{2e})\theta_1^{\text{SH}}M_1J_3^c$. It says that, due to the interaction between the charge current and magnetization, the charge current generates a spin current of polarization along the magnetization and flowing direction along the charge current, as shown in Fig. 5(d).

In the current work, these principally allowed new SHEs and ISHEs in magnetic materials have not been considered. It is expected that the new effects are higher orders in comparison with the usual SHE and ISHE because they involve both spin-orbit interaction and charge-magnon interactions. Nevertheless, it shall be very interesting to experimentally confirm these predictions although they must exist.

IV. CONCLUSIONS

In conclusion, a careful analysis of the electrical signals of the st-FMR in a HM/FM bilayer has been carried out. Both rf Oersted field and rf SOTs, which cause the ferromagnetic resonance, are considered in the analysis. Differ from previous studies on the st-FMR, the tensor nature of the dynamical susceptibilities is also included. It is shown that one can indeed use dc-voltage line shape and the angular dependence of dc voltage to actually extract spin-Hall angle of the HM besides other typical magnetic material parameters in a traditional FMR measurement.

ACKNOWLEDGMENTS

This work was supported by the National Natural Science Foundation of China (Grants No. 11774296, No. 51571109, and No. 11734006), Hong Kong RGC Grants No. 16301816, No. 1631518, and No. 16300117, as well as the National Key R&D Program of China (Grants No. 2017YFA0303202 and No. 2018YFA0306004). HFD acknowledges the support of China Scholarship Council (CSC), Colorado State University (CSU) during his stay in CSU, and the Fundamental Research Funds for the Central Universities (Grants No. 14380104 and No. 14380078).

- [1] C. Kittel, *Phys. Rev.* **73**, 155 (1948).
- [2] D. Polder, *Philos. Mag.* **40**, 99 (1949).
- [3] H. Suhl, *Phys. Rev.* **97**, 555 (1955).
- [4] P. E. Tannenwald, *Phys. Rev.* **100**, 1713 (1955).
- [5] H. Seidel and H. Boyet, *J. Appl. Phys.* **28**, 452 (1957).
- [6] B. Lax and K. J. Button, *Microwave Ferrites and Ferrimagnetics* (New York, McGraw-Hill, 1962).
- [7] M. Farle, *Rep. Prog. Phys.* **61**, 755 (1998).
- [8] E. Schlomann, *J. Phys. Chem. Solids* **6**, 257 (1958).
- [9] V. A. Ignatchenko and V. A. Felk, *Phys. Rev. B* **71**, 094417 (2005).
- [10] Z. Celinski and B. Heinrich, *J. Appl. Phys.* **70**, 5935 (1991).
- [11] B. A. Belyaev, A. V. Izotov, and A. L. Leksikov, *IEEE Sensors J.* **5**, 260 (2005).
- [12] C. Vittoria, *Magnetics, Dielectrics and Wave Propagation with MAT/LAB Codes* (CRC Press, New York, 2010).
- [13] G. Counil, J.-V. Kim, T. Devolder, P. Crozat, C. Chappert, and A. Cebollada, *J. Appl. Phys.* **98**, 023901 (2005).
- [14] H. J. Juretschke, *J. Appl. Phys.* **31**, 1401 (1960).
- [15] W. G. Egan and H. J. Juretschke, *J. Appl. Phys.* **34**, 1477 (1963).
- [16] M. Harder, Z. X. Cao, Y. S. Gui, X. L. Fan, and C.-M. Hu, *Phys. Rev. B* **84**, 054423 (2011).
- [17] E. Saitoh, M. Ueda, H. Miyajima, and G. Tatara, *Appl. Phys. Lett.* **88**, 182509 (2006).

- [18] K. Ando, S. Takahashi, J. Ieda, Y. Kajiwara, H. Nakayama, T. Yoshino, K. Harii, Y. Fujikawa, M. Matsuo, S. Maekawa, and E. Saitoh, *J. Appl. Phys.* **109**, 103913 (2011).
- [19] M. V. Costache, M. Sladkov, S. M. Watts, C. H. van der Wal, and B. J. van Wees, *Phys. Rev. Lett.* **97**, 216603 (2006).
- [20] O. Mosendz, J. E. Pearson, F. Y. Fradin, G. E. W. Bauer, S. D. Bader, and A. Hoffmann, *Phys. Rev. Lett.* **104**, 046601 (2010).
- [21] L. Liu, T. Moriyama, D. C. Ralph, and R. A. Buhrman, *Phys. Rev. Lett.* **106**, 036601 (2011).
- [22] W. Zhang, W. Han, X. Jiang, S.-H. Yang, and Stuart S. P. Parkin, *Nature Physics* **11**, 496 (2015).
- [23] T. Nan, S. Emori, C. T. Boone, X. Wang, T. M. Oxholm, J. G. Jones, B. M. Howe, G. J. Brown, and N. X. Sun, *Phys. Rev. B* **91**, 214416 (2015).
- [24] Y. Wang, P. Deorani, X. Qiu, J. H. Kwon, and H. Yang, *Appl. Phys. Lett.* **105**, 152412 (2014).
- [25] K. Kondou, H. Sukagawa, S. Mitani, K. Tsukagoshi, and S. Kasai, *Appl. Phys. Express* **5**, 073002 (2012).
- [26] A. Azevedo, L. H. Vilela-Leão, R. L. Rodríguez-Suárez, A. F. Lacerda Santos, and S. M. Rezende, *Phys. Rev. B* **83**, 144402 (2011).
- [27] H. Nakayama, K. Ando, K. Harii, T. Yoshino, R. Takahashi, Y. Kajiwara, K. Uchida, Y. Fujikawa, and E. Saitoh, *Phys. Rev. B* **85**, 144408 (2012).
- [28] Z. Feng, J. Hu, L. Sun, B. You, D. Wu, J. Du, W. Zhang, A. Hu, Y. Yang, D. M. Tang, B. S. Zhang, and H. F. Ding, *Phys. Rev. B* **85**, 214423 (2012).
- [29] L. Chen, S. Ikeda, F. Matsukura, and H. Ohno, *Appl. Phys. Express* **7**, 013002 (2014).
- [30] Y. S. Gui, N. Mecking, X. Zhou, Gwyn Williams, and C.-M. Hu, *Phys. Rev. Lett.* **98**, 107602 (2007).
- [31] A. A. Tulapurkar, Y. Suzuki, A. Fukushima, H. Kubota, H. Maehara, K. Tsunekawa, D. D. Djayaprawira, N. Watanabe, and S. Yuasa, *Nature (London)* **438**, 339 (2005).
- [32] J. C. Sankey, P. M. Braganca, A. G. F. Garcia, I. N. Krivorotov, R. A. Buhrman, and D. C. Ralph, *Phys. Rev. Lett.* **96**, 227601 (2006).
- [33] S. T. B. Goennenwein, S. W. Schink, A. Brandlmaier, A. Boger, M. Opel, R. Gross, R. S. Keizer, T. M. Klapwijk, A. Gupta, H. Huebl, C. Bihler, and M. S. Brandt, *Appl. Phys. Lett.* **90**, 162507 (2007).
- [34] A. Yamaguchi, H. Miyajima, T. Ono, Y. Suzuki, S. Yuasa, A. Tulapurkar, and Y. Nakatani, *Appl. Phys. Lett.* **90**, 182507 (2007).
- [35] Y. Zhang, X. S. Wang, H. Y. Yuan, S. S. Kang, H. W. Zhang, and X. R. Wang, *J. Phys.: Condens. Matter* **29**, 095806 (2017).
- [36] X. Tao, Q. Liu, B. Miao, R. Yu, Z. Feng, L. Sun, B. You, J. Du, K. Chen, S. Zhang, L. Zhang, Z. Yuan, D. Wu, and H. Ding, *Sci. Adv.* **4**, eaat1670 (2018).
- [37] M. B. Jungfleisch, A. V. Chumak, A. Kehlberger, V. Lauer, D. H. Kim, M. C. Onbasli, C. A. Ross, M. Kläui, and B. Hillebrands, *Phys. Rev. B* **91**, 134407 (2015).
- [38] S. Mizukami, Y. Ando, and T. Miyazaki, *Phys. Rev. B* **66**, 104413 (2002).
- [39] Y. Sun, H. Chang, M. Kabatek, Y.-Y. Song, Z. Wang, M. Jantz, W. Schneider, M. Wu, E. Montoya, B. Kardasz, B. Heinrich, S. G. E. te Velthuis, H. Schultheiss, and A. Hoffmann, *Phys. Rev. Lett.* **111**, 106601 (2013).
- [40] J. E. Hirsch, *Phys. Rev. Lett.* **83**, 1834 (1999).
- [41] Y. Tserkovnyak, A. Brataas, and G. E. W. Bauer, *Phys. Rev. Lett.* **88**, 117601 (2002).
- [42] Y. Tserkovnyak, A. Brataas, G. E. W. Bauer, and B. I. Halperin, *Rev. Mod. Phys.* **77**, 1375 (2004).
- [43] A. Manchon and S. Zhang, *Phys. Rev. B* **79**, 094422 (2009).
- [44] B. F. Miao, S. Y. Huang, D. Qu, and C. L. Chien, *Phys. Rev. Lett.* **112**, 236601 (2014).
- [45] T. Chiba, M. Schreier, G. E. W. Bauer, and S. Takahashi, *J. Appl. Phys.* **117**, 17C715 (2015).
- [46] M. Schreier, T. Chiba, A. Niedermayr, J. Lotze, H. Huebl, S. Geprägs, S. Takahashi, G. E. W. Bauer, R. Gross, and S. T. B. Goennenwein, *Phys. Rev. B* **92**, 144411 (2015).
- [47] J. C. Slonczewski, *J. Magn. Magn. Mater.* **159**, L1 (1996).
- [48] L. Berger, *Phys. Rev. B* **54**, 9353 (1996).
- [49] T. L. Gilbert, *IEEE Trans. Magn.* **40**, 3443 (2004).
- [50] Y. Zhang, H. W. Zhang, and X. R. Wang, *Europhys. Lett.* **113**, 47003 (2016).